Laser-driven direct quantum control of nuclear excitations

Ian Wong,* Andreea Grigoriu, Jonathan Roslund, Tak-San Ho, and Herschel Rabitz
Department of Chemistry, Princeton University, Princeton, New Jersey 08544, USA
(Received 9 September 2011; published 23 November 2011)

The possibility of controlled direct laser-nuclear excitations is considered from a quantum control perspective. The controllability of laser-driven electric dipole and magnetic dipole transitions among pure nuclear states is analyzed. Within a set of realistic and general conditions, atomic nuclei are demonstrated to possess full state controllability. Additionally, an analysis of the nuclear state excitation probability as a function of the laser control field is conducted. This control landscape is shown to possess a generic topology, which has important physical consequences for achieving optimal nuclear state excitation with laser fields. Last, an assessment is given of the technological challenges that need to be considered when implementing direct nuclear control in the laboratory.

DOI: 10.1103/PhysRevA.84.053429 PACS number(s): 32.80.Qk, 25.20.−x, 42.50.−p, 42.55.Vc

I. INTRODUCTION

The control of nuclear dynamics with high-intensity lasers has been a long-standing objective [1,2]. Recent experiments for this purpose have relied upon *indirect* methods of nuclear excitation, including the use of laser-accelerated electron and proton beams or Bremsstrahlung radiation produced from laser-generated plasmas [3]. *Direct* laser-nuclear excitation has thus far been prohibitive due to both a lack of coherent photon sources matching typical nuclear transition energies and the enormous laser intensities required to overcome the inherently small nuclear excitation cross sections [1]. However, with the future development of high-intensity, coherent x-ray sources [4], direct laser-driven nuclear dynamics may become practical.

An important objective is to determine the feasibility of coherent radiation-driven nuclear dynamics, in analogy to that achieved at the atomic and molecular scales. Optimally shaped ultrafast laser fields have been demonstrated to coherently alter the quantum dynamics of complex atomic and molecular species in a multitude of applications [5–11]. As the prospects for the study of direct laser-nuclear dynamics continue to improve, the possible extension of these quantum control concepts to the nuclear domain deserves careful consideration.

This paper explores direct laser-driven quantum nuclear control from a theoretical perspective. The laser-nuclear interaction and Schrödinger equation within the dipole approximation are described in Sec. II. The state controllability of nuclear quantum systems is investigated in Sec. III to establish, in principle, the ability to freely manipulate the laser-induced nuclear transition probability from an arbitrary initial state to an arbitrary final state. The control landscape is defined as the transition probability as a functional of the applied field; the topology of the landscape is important for the efficiency of finding effective controls. The landscape is shown in Sec. IV to have a generic topology for laser-driven nuclear excitations. In addition, the Hessian of the nuclear transition probability, with respect to the applied field at an optimum, is investigated together with an assessment of the physical consequences of its properties. Finally, practical aspects of performing direct nuclear quantum control experiments are considered in Sec. V. In this regard, the applicability of laser-pulse-shaping techniques, evolutionary learning algorithms, and nuclear acceleration is considered along with prospective technological developments favorable for the realization of the proposed nuclear control schemes.

II. LASER-NUCLEAR INTERACTION DYNAMICS

The atomic nucleus is a complex many-body system that does not possess a center of attraction, as is experienced by electrons in atoms, yet nuclear structure still exhibits many qualitative similarities to atomic structure. In particular, the nucleus can be effectively described by a series of quantized energy levels that fill with neutrons and protons according to the Pauli exclusion principle [12,13]. Additionally, nuclei possess a series of unoccupied, energetically excited states above the stable ground state into which nucleons may be promoted through their interaction with electromagnetic radiation. The controllability and control landscape topology analyses presented in Secs. III and IV, respectively, examine the ability to arbitrarily manipulate transitions among such states. Importantly, these assessments are not dependent upon the specific internal structure of the nucleus (e.g., the particular form of the nuclear potential); rather, the present analyses require only a general model for the atomic nucleus consisting of a series of stable, bound nuclear energy levels coupled by electromagnetically induced transitions. The Hamiltonian describing the nucleus and its interaction with an external electromagnetic field can be expressed as

$$H(t) = H_0 + H_1(t), \tag{1}$$

where H_0 represents the internal Hamiltonian of the nucleus and $H_1(t)$ describes its coupling with the applied laser field (see [12] for more details).

While typical nuclear binding energies are on the order of 10^6 eV per nucleon, transition energies among bound nuclear levels are generally on the order of 10^3–10^5 eV [14]. Currently planned free-electron x-ray laser sources are expected to possess photon energies of at most $h\nu \sim 10^4$ eV, which are insufficient for inducing nuclear fission or photodisintegration [13,15]. Consequently, only relatively low-energy transitions

*iwong@princeton.edu

among bound excited states are considered in this paper. The present work considers the nucleus as a finite N-level quantum system described by the internal Hamiltonian $H_0 = \sum_{n=1}^{N} \lambda_n |n\rangle\langle n|$ with eigenstates $|n\rangle : n = 1, \ldots, N$, and corresponding energy spectrum $\{\lambda_n\}$.

A stable nucleus of approximately constant density exhibits a radius R empirically determined as $R \simeq r_0 A^{1/3}$, where $r_0 = 1.25 \times 10^{-15}$ m and A is the atomic mass number. Currently envisioned high-energy laser beam sources capable of direct nuclear interaction have wavelengths on the order of 10^{-10} m. For a nucleus with mass number $A = 100$, the nuclear radius is approximately 6×10^{-15} m, and thus, any spatial variation of the field with respect to the nucleus may be neglected. Upon considering contributions from both the electric and magnetic components of the applied laser field, the interaction Hamiltonian $H_1(t)$ may be expressed within the dipole approximation as

$$H_1(t) = -\boldsymbol{\mu}_1 \cdot \boldsymbol{\epsilon}_1(t) - \boldsymbol{\mu}_2 \cdot \boldsymbol{\epsilon}_2(t), \tag{2}$$

where the electric dipole $\boldsymbol{\mu}_1$ and magnetic dipole $\boldsymbol{\mu}_2$ interact, respectively, with the electric $\boldsymbol{\epsilon}_1(t)$ and magnetic $\boldsymbol{\epsilon}_2(t)$ components of the applied laser field. The magnetic dipole operator $\boldsymbol{\mu}_2$ includes contributions from both the orbital motion and the intrinsic spin of each nucleon, which enables the interaction of the laser pulse with the uncharged neutron. The resulting electric dipole and magnetic dipole transitions among the nuclear levels are denoted as $E1$ and $M1$, respectively. For a typical nucleon charge separation distance on the order of 10^{-15} m, the transition electric dipole moment is on the order of 10^{-34} C m; the corresponding interaction energy with the nuclear electric dipole is $E_E \simeq 1.7 \times 10^{-12} I^{1/2}$ eV, where the pulse peak intensity I is given in W/cm^2. Likewise, assuming a magnetic dipole on the order of the nuclear magneton μ_N, the magnetic interaction energy is $E_M \simeq 2.9 \times 10^{-13} I^{1/2}$ eV. Hence, the nuclear electric and magnetic dipole couplings are approximately of the same order. However, even for very high laser intensities ($I \sim 10^{21}$ W/cm^2), the field couples to the nucleus in a weak manner and does not significantly perturb the field-free structure.

Nuclear eigenstates are generally characterized by both total angular momentum J and quantum parity π, which corresponds to either even ($\pi = +1$) or odd ($\pi = -1$) values of the orbital angular momentum L. Electric dipole ($E1$) transitions (with a selection rule of $\Delta L = \pm 1$) exhibit a parity-conservation rule of $\pi_i \pi_f = -1$, while magnetic dipole ($M1$) transitions ($\Delta L = 0$) display a parity-conversation rule of $\pi_i \pi_f = +1$ [13]. Accordingly, $E1$ and $M1$ transitions between nuclear eigenstates are mutually exclusive. Nuclei also exhibit collective motions, such as surface vibrations and rotations, which lead to a rich array of quantized sublevels. For the present analysis of laser-driven transitions between energetically distinct (J,π) states, the sublevel splittings of each individual shell are not considered.

In the present application of controlled nuclear excitation, we consider the transition probability $P_{i\to f}$ between an initial state $|\psi_i\rangle$ and a final state $|\psi_f\rangle$, both of which are pure states of the field-free nuclear Hamiltonian H_0; these states may either be eigenstates $|n\rangle$ of the Hamiltonian H_0 or superposition states $|\psi\rangle = \sum_{n=1}^{N} a_n |n\rangle$, where the complex coefficients a_n satisfy the normalization condition $\sum_{n=1}^{N} |a_n|^2 = 1$, with N being the total number of accessible states.

While a more general density matrix analysis allows for the possibility of mixed states, the characteristic shell energy spacings of nuclei in thermodynamic equilibrium prevent the construction of mixed nuclear states under normal conditions, except in the cases of particle collisions and decay, which are beyond the scope of the present work [13]. Hence, the subsequent analyses examine the ability to control transitions among pure nuclear states with coherent laser radiation.

The time evolution of a pure nuclear state is described by the Schrödinger equation

$$i\hbar \frac{\partial |\psi(t)\rangle}{\partial t} = [H_0 - \boldsymbol{\mu}_1 \cdot \boldsymbol{\epsilon}_1(t) - \boldsymbol{\mu}_2 \cdot \boldsymbol{\epsilon}_2(t)]|\psi(t)\rangle, \tag{3}$$

which will serve as the governing dynamical equation for the analyses and assessments in this paper. For simplicity, linear polarization of the transverse electromagnetic field is assumed, which allows Eq. (3) to be recast as

$$i\hbar \frac{\partial |\psi(t)\rangle}{\partial t} = [H_0 - \mu_1 \epsilon_1(t) - \mu_2 \epsilon_2(t)]|\psi(t)\rangle. \tag{4}$$

III. CONTROLLABILITY ANALYSIS

This section analyzes the controllability of laser-driven nuclear excitation by extending the graph theory approach [16] originally developed for treating atomic and molecular systems. Nuclear state controllability seeks to establish the existence of a set of laser control fields $\epsilon_1(t)$ and $\epsilon_2(t)$ that are capable of steering the quantum system from an arbitrary initial state $|\psi(0)\rangle = |\psi_i\rangle$ to an arbitrary final state $|\psi(T)\rangle = |\psi_f\rangle$ at a target time T [16]. The necessary and sufficient conditions for state controllability are considered, along with a few specific examples.

A. Conditions for state controllability

To facilitate the controllability analysis, we associate with the system a nonoriented connectivity graph $\mathcal{G} = (\mathcal{V},\mathcal{E})$. The set of vertices $\mathcal{V}$ of the graph is defined as the collection of eigenstates $|n\rangle$ of the field-free Hamiltonian H_0, and the set of edges $\mathcal{E}$ is composed of all pairs of eigenstates coupled by the dipole matrix elements of μ_1 and μ_2:

$$\begin{aligned} &\mathcal{G} = (\mathcal{V},\mathcal{E}) : \mathcal{V} = \{|n\rangle, i = 1,...,N\}, \\ &\mathcal{E} = \{(|a\rangle,|b\rangle); |a\rangle \neq |b\rangle, \mu_{ab} \neq 0 \ \text{ for some } \ \mu \in \{\mu_1,\mu_2\}\}. \end{aligned} \tag{5}$$

An example of such a graph is shown in Fig. 1 for the nine lowest eigenstates of the nucleus $^{153}_{63}$Eu. The vertices (eigenstates of the field-free Hamiltonian H_0) are represented by horizontal lines along with the corresponding energy λ_n relative to the nuclear ground state; all energy values and dipole couplings ($E1$ and $M1$) are taken from the Evaluated Nuclear Structure Data File (ENSDF) database [17]. The graph edges are depicted by arrows connecting various eigenstates. Since the $E1$ and $M1$ transitions are mutually exclusive, two distinct types of edges exist, as explicitly seen in Fig. 1.

Denoting the transition energy between the eigenstates $|i\rangle$ and $|j\rangle$ as $\omega_{ij} = |\lambda_i - \lambda_j|$, $i,j = 1,...,N$, the nuclear system dynamically governed by Eq. (4) is controllable under the

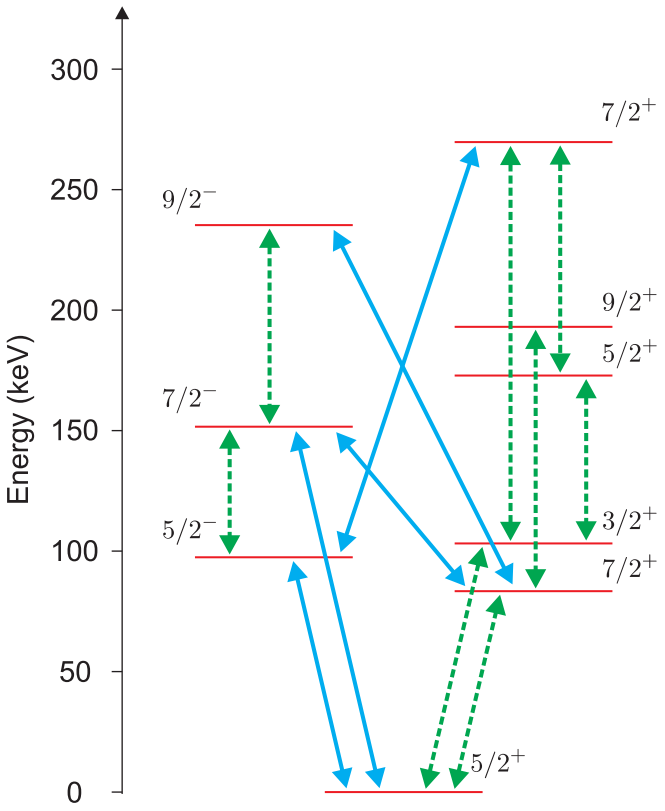

FIG. 1. (Color online) Representation of the connectivity graph for the nine lowest excited eigenstates of $^{153}_{63}$Eu [17]. Of the observed eigenstates below 300 keV, only dipole-allowed transitions contributing at least 5% of the total emissive oscillator strength from a given state are included in the connectivity graph. The vertices $\mathcal{V}$ of the connectivity graph correspond to the nuclear eigenstates, represented by horizontal lines, along with their associated energy and term symbol. Arrows connecting the various eigenstates are the graph edges $\mathcal{E}$; $E1$ transitions are depicted by blue solid arrows, and $M1$ transitions are depicted by green dashed arrows.

following conditions: (i) $\mathcal{C}_1$, the graph $\mathcal{G}$ is connected, and (ii) $\mathcal{C}_2$, the graph $\mathcal{G}$ does not have degenerate transitions, i.e., for every $(i,j) \neq (a,b)$, $i \neq j$, $a \neq b$ such that $\mu_{ij} \neq 0$, $\mu_{ab} \neq 0$, for some $\mu \in \{\mu_1,\mu_2\}$: $\omega_{ij} \neq \omega_{ab}$. In the present scenario, the electric dipole and magnetic dipole interaction matrices, μ_1 and μ_2, are nonoverlapping (i.e., element-by-element multiplication of μ_1 and μ_2 yields a zero matrix due to parity-selection rules). Consequently, the proof of this controllability statement follows the same steps as that for the atomic and molecular cases in which only the electric dipole interaction is considered [16].

The first condition $\mathcal{C}_1$ determining state controllability implies that at least one connected path exists between any two vertices $|i\rangle$ and $|j\rangle$. Thus, any eigenstate must be connected to every other eigenstate under consideration by means of $E1$ and/or $M1$ transitions (with no regard for how many intermediate eigenstates lie along the connecting path). Condition $\mathcal{C}_1$ is necessary for controllability, while condition $\mathcal{C}_2$ is only sufficient since there are systems with degenerate transitions that can be proven controllable (see [16] for more details).

B. Evaluation of controllability

As a demonstration of state controllability, the case of $^{153}_{63}$Eu is assessed by examining the connectivity graph in Fig. 1. A set of edges exist that allow for movement from any initial vertex to every other vertex. Accordingly, the graph $\mathcal{G}$ for $^{153}_{63}$Eu is connected. It is also clear from Fig. 1 that the graph contains no degenerate transitions. Since both conditions for controllability are satisfied, the nuclear system $^{153}_{63}$Eu is state controllable.

State controllability can be readily determined in a systematic fashion utilizing the above graphical methodology. Several nuclei with an odd number of nucleons in the actinide and lanthanide series of the periodic table were examined. Nuclei belonging to these groups are of particular interest since they typically possess an energetically low-lying excited state that may be directly accessed with available laser sources. For instance, the lowest dipole-accessible excited states for $^{151}_{62}$Sm, $^{169}_{69}$Tm, $^{171}_{69}$Tm, and $^{201}_{80}$Hg are each below 10 keV [17]. The narrow bandwidths ($\sim$0.1% of the photon energy) and limited field strengths of existing x-ray laser sources (see Sec. V) place a practical limit on the number of relevant states; for the purpose of analyzing controllability, only excited states lying below an excitation energy of 300 keV were considered for the following nuclei: $^{151}_{62}$Sm(13), $^{151}_{63}$Eu(3), $^{153}_{63}$Eu(8), $^{161}_{66}$Dy(10), $^{167}_{69}$Tm(9), $^{169}_{69}$Tm(2), $^{171}_{69}$Tm(2), and $^{201}_{80}$Hg(4). The numeric value in parentheses denotes the number of dipole-accessible excited states considered in the analysis. Upon applying the two controllability conditions $\mathcal{C}_1$ and $\mathcal{C}_2$, each of these nuclear systems was found to be state controllable.

The expected general controllability of nuclei follows from state connectivity and the typical absence of degeneracy in their energy spectra [13,14]. It is important to note that degeneracy in the present circumstance does not refer to magnetic sublevels M_J corresponding to a single total angular momentum state J, but rather to the notion of two physically distinct (J,π) states of the same energy. Moreover, as the Hilbert space dimension N increases, it has been demonstrated that a larger fraction of states should be connected [18]. As a result, upon including higher-energy excited states in the controllability analysis, it is expected that a nucleus that has already been established as connected will remain so. Accordingly, with the exception of cases possessing accidental degeneracy, full state controllability is expected to be a general feature of laser-driven nuclear excitation.

IV. NUCLEAR CONTROL LANDSCAPE TOPOLOGY

When a nucleus is state controllable, the external fields $\epsilon_1(t)$ and $\epsilon_2(t)$ may be appropriately varied to freely manipulate the transition probability $P_{i\to f}$. The control landscape is defined as $P_{i\to f}$ as a functional of the control fields:

$$P_{i\to f} = P_{i\to f}[\epsilon_1(t),\epsilon_2(t)]. \tag{6}$$

The maximization of the transition probability entails a search for the controls $\epsilon_1(t)$ and $\epsilon_2(t)$ over this landscape. In the laboratory, technological limitations will generally introduce significant constraints on the controls; further details concerning the experimental aspects of this effort are presented in Sec. V. Notwithstanding the technological circumstances, the

goal here is to assess the topology of the control landscape in the idealized limit where control resources are fully available. An *a priori* expectation is that the control landscape would have a highly complex topology, with possibly many maxima, minima, and saddle points. In particular, it is reasonable to expect the existence of suboptimal local maxima where $P_{i\to f} < 1$, which can act as traps in laboratory searches for optimal control fields [19]. Hence, an understanding of the topological features of the landscape is of prime interest. In this section, an analysis of the control landscape topology for nuclear transitions is given, expanding on earlier work done in [20,21] to account for the presence of both electric $\epsilon_1(t)$ and magnetic $\epsilon_2(t)$ fields. We investigate the properties of the gradient of the landscape with respect to the fields, the possible existence of suboptimal maxima, and the behavior of the landscape Hessian around the global maximum $P_{i\to f} = 1.0$, along with the physical consequences of these properties.

A. Control landscape formulation: Gradient analysis of $P_{i\to f}$

The control landscape for a laser-driven nucleus is given by [20]

$$P_{i\to f} = |\langle\psi_f|U(T,0)|\psi_i\rangle|^2, \tag{7}$$

where the unitary time evolution operator $U(t,0)$ satisfies

$$i\hbar\frac{\partial U(t,0)}{\partial t} = [H_0 - \epsilon_1(t)\mu_1 - \epsilon_2(t)\mu_2]U(t,0), \tag{8}$$

with the state evolving as $|\psi(t)\rangle = U(t,0)|\psi_i\rangle$.

Maximization of the transition probability entails climbing the landscape until a critical point is reached where the gradient of $P_{i\to f}$ with respect to the fields $\epsilon_1(t)$ and $\epsilon_2(t)$ is zero. A critical point could correspond to a local maximum, minimum, or saddle on the transition probability landscape as well as the global minimum and the desired global maximum value. The condition for the landscape gradient to vanish is given by (see [21] for more details)

$$\frac{\delta P_{i\to f}}{\delta\epsilon_m(t)} = \frac{2}{\hbar}\mathrm{Im}[\langle\psi_i|\mu_m(t)|q\rangle] = 0, \quad \forall\, t > 0, \quad m = 1,2, \tag{9}$$

where $|q\rangle = U^\dagger(T,0)|\psi_f\rangle\langle U(T,0)|\psi_i\rangle$ and $\mu_m(t) = U^\dagger(t,0)\mu_m U(t,0)$ is the evolution of the dipole operator. It has been shown [20] that only control fields corresponding to $P_{i\to f} = 1.0$ and $P_{i\to f} = 0$ satisfy the condition in Eq. (9). Thus, the control landscape for a laser-driven nucleus only possesses critical points associated with perfect or null control. In particular, there are no unconstrained control fields that produce suboptimal critical points in the landscape corresponding to transition probabilities $0 < P_{i\to f} < 1.0$. The important consequence of this conclusion is that searches with adequate freedom for the fields within the dipole approximation should not encounter suboptimal traps in the transition probability landscape.

Under realistic laboratory conditions, there can be constraints on the feasible values for the target time T and especially the ability to arbitrarily sculpt the laser fields. While these circumstances do not detract from the theoretically deduced controllability and landscape topology analyses presented here, they can have important physical consequences in realistic laboratory studies of nuclear control. An upper limit on the target time stems from the finite lifetime of excited nuclear states, which imposes a long-time limit on the coherent control among states. In addition, if the coherence time of the laser pulse is shorter than the lifetime of the excited state, the effective upper limit on T is further diminished. Fundamentally, the target time also needs to be sufficiently long to permit attaining full controllability. The generation of the control fields is always encumbered by practical considerations in the laboratory, which are discussed in Sec. V. Significant constraints on the controls can lead to artificial suboptimal traps in the nominally trap-free landscape. Nevertheless, numerical simulations [22] have shown that, even with modest constraints in the controls, extremely high transition yields ($P_{i\to f} > 0.90$) are achievable in many cases.

B. Analysis of stability and robustness upon seeking optimal control fields

The overall success of a laboratory search is greatly influenced by both the climb over the landscape toward an optimal solution and the search landscape topology in the immediate vicinity of an optimal solution [20]. In this regard, we first consider the magnitude of the landscape slope $\delta P_{i\to f}/\delta\epsilon_m$ on the way toward an extremum.

An upper bound for $\delta P_{i\to f}/\delta\epsilon_m$ can be established using Eq. (9):

$$\left\|\frac{\delta P_{i\to f}}{\delta\epsilon_m(t)}\right\| = \frac{2}{\hbar}\|\mathrm{Im}[\langle\psi_i|U^\dagger(t,0)\mu_m U(t,0)|q\rangle]\| \leqslant \frac{2}{\hbar}\|\mu_m\|, \quad m = 1,2. \tag{10}$$

In any practical application, the norms of the dipole operators μ_1 and μ_2 are always finite. Thus, the landscape slope on the way toward an extremum is rather gentle, without any steep regions, thereby assuring stability in the search (see [21] for more discussion). This stability to noise is important for climbing the landscape, regardless of the nature of the algorithm utilized.

Upon arriving at the landscape maximum, the topology of the landscape in that region is important for assessing the robustness of the optimal solution to noise and other errors in the controls. Toward this end, a detailed examination of the Hessian at $P_{i\to f} = 1.0$ is required. In this case, the Hessian is defined by a matrix composed of four Hermitian submatrices of infinite dimension over the domain $[0,T]$:

$$\mathcal{H}(t,t') = \begin{pmatrix} \mathcal{H}_{11}(t,t') & \mathcal{H}_{12}(t,t') \\ \mathcal{H}_{21}(t,t') & \mathcal{H}_{22}(t,t') \end{pmatrix}, \tag{11}$$

where the matrix elements are given by

$$\mathcal{H}_{mn}(t,t') = \frac{\delta^2 P_{i\to f}}{\delta\epsilon_m(t)\delta\epsilon_n(t')} \quad \text{for} \quad m,n = 1,2. \tag{12}$$

The Hessian is real and symmetric, with the matrix elements satisfying the relations $\mathcal{H}_{mn}(t,t') = \mathcal{H}_{mn}(t',t)$ and $\mathcal{H}_{mn}(t,t') = \mathcal{H}_{nm}(t,t')$ for $m,n = 1,2$. Following prior work for a single control field [20], the upper triangular matrix portions (i.e.,

$t \geqslant t'$) of all four submatrices of the Hessian can be expressed as

$$\mathcal{H}_{mn}(t,t') = -\frac{2}{\hbar^2}\mathrm{Re}(\langle\psi_i|\{[\mu_m(t) - \langle\psi_i|\mu_m(t)|\psi_i\rangle] \times [\mu_n(t') - \langle\psi_i|\mu_n(t')|\psi_i\rangle]\}|\psi_i\rangle), \; t \geqslant t'. \quad (13)$$

In a similar fashion, the diagonal elements of the full Hessian can be evaluated as

$$\begin{aligned}\mathcal{H}_{mm}(t,t) &= \frac{\delta^2 P_{i\to f}}{\delta[\epsilon_m(t)]^2} \\ &= -\frac{2}{\hbar^2}\langle\psi_i|[\mu_m(t) - \langle\psi_i|\mu_m(t)|\psi_i\rangle]^2|\psi_i\rangle \\ &\geqslant -\frac{2}{\hbar^2}\|\mu_m^2\|, \quad m = 1,2. \end{aligned} \quad (14)$$

From the last relation, it follows that the trace of the Hessian is bounded from below,

$$\mathrm{tr}(\mathcal{H}) = \sum_{m=1}^{2}\int_0^T \mathcal{H}_{mm}(t,t)dt \geqslant -\frac{2T}{\hbar^2}\sum_{m=1}^{2}\|\mu_m^2\|, \quad (15)$$

which has important physical significance, which will be discussed later.

The Hessian in Eq. (11) has an infinite set of eigenvalues σ_k and corresponding eigenvectors $\mathbf{u}_k(t) = (u_k^{(1)}(t), u_k^{(2)}(t))$ that satisfy the following equation [21]:

$$\sum_{n=1}^{2}\int_0^T \mathcal{H}_{mn}(t,t')u_k^{(n)}(t')dt' = \sigma_k u_k^{(m)}(t), \quad m = 1,2. \quad (16)$$

At the landscape global maximum, each of the four submatrices of the Hessian in Eq. (13) can be reexpressed as a symmetric and separable kernel of the form

$$\mathcal{H}_{mn}(t,t') = -\frac{2}{\hbar^2}\sum_{k'=1}^{2N-2}\phi_{k'}^{(m)}(t)\phi_{k'}^{(n)}(t'), \quad m,n = 1,2, \quad (17)$$

by utilizing the dual $(2N-2)$-dimensional bases $\boldsymbol{\phi}_{k'}(t) = (\phi_{k'}^{(1)}(t), \phi_{k'}^{(2)}(t))$, whose component functions are

$$\begin{aligned}\{\phi_{k'}^{(m)}(t)\} = \{&\mathrm{Re}[\xi_1^{(m)}(t)], \mathrm{Im}[\xi_1^{(m)}(t)], \ldots, \\ &\mathrm{Re}[\xi_{N-1}^{(m)}(t)], \mathrm{Im}[\xi_{N-1}^{(m)}(t)]\}, \quad m = 1,2,\end{aligned} \quad (18)$$

where $\xi_l^{(m)}(t) = \langle l|\mu_m(t)|\psi_i\rangle$ with $|l\rangle \neq |\psi_i\rangle$ for all l [20]. It follows from Eq. (17) that the Hessian at the landscape maximum is finite rank (i.e., possesses a finite subset of nonzero eigenvalues along with infinitely many zero eigenvalues).

Upon substituting Eq. (17) into Eq. (16) and denoting $w_{k'k} = \sum_{n=1}^{2}\int_0^T \phi_{k'}^{(n)}(t')u_k^{(n)}(t')dt'$, the Hessian eigenvalue equation reduces to

$$-\frac{2}{\hbar^2}\sum_{k'=1}^{2N-2}\phi_{k'}^{(m)}(t)w_{k'k} = \sigma_k u_k^{(m)}(t), \quad m = 1,2. \quad (19)$$

After multiplying by $\phi_{k''}^{(m)}(t)$, integrating with respect to time, and summing over m, we get

$$\begin{aligned}-\frac{2}{\hbar^2}\sum_{k'=1}^{2N-2}\left[\sum_{m=1}^{2}\int_0^T \phi_{k''}^{(m)}(t)\phi_{k'}^{(m)}(t)dt\right]w_{k'k} \\ = \sigma_k\left[\sum_{m=1}^{2}\int_0^T \phi_{k''}^{(m)}(t)u_k^{(m)}(t)dt\right].\end{aligned} \quad (20)$$

Now, defining $A_{k''k'} = -\frac{2}{\hbar^2}\sum_{m=1}^{2}\int_0^T \phi_{k''}^{(m)}(t)\phi_{k'}^{(m)}(t)dt$, we can simplify Eq. (20) to give

$$\sum_{k'=1}^{2N-2}A_{k''k'}w_{k'k} = \sigma_k w_{k''k}, \quad 1 \leqslant k \leqslant 2N-2. \quad (21)$$

Consolidating the indexes and rewriting the expression in matrix notation, we arrive at $2N-2$ distinct eigenvalue equations:

$$\mathbf{A}\cdot\mathbf{w}_k = \sigma_k\mathbf{w}_k, \quad 1 \leqslant k \leqslant 2N-2. \quad (22)$$

By interchanging the indexes k'' and k' in the definition of $A_{k''k'}$, it is clear that the $(2N-2)\times(2N-2)$ matrix $\mathbf{A}$ is symmetric; furthermore, the diagonal elements $A_{k'k'} = -\frac{2}{\hbar^2}\sum_{m=1}^{2}\int_0^T dt\,[\phi_{k'}^{(m)}(t)]^2$ are all negative. This means that $\mathbf{A}$ can be transformed into a congruent diagonal matrix containing only nonpositive diagonal entries. It follows from Sylvester's law of inertia that the $2N-2$ eigenvalues σ_k of $\mathbf{A}$ must be nonpositive. Thus, the Hessian $\mathcal{H}(t,t')$ at the landscape maximum possesses *at most* $2N-2$ nonzero, negative eigenvalues $\sigma_1, \sigma_2, \ldots, \sigma_{2N-2}$ associated with $2N-2$ orthonormal eigenvectors $\mathbf{u}_1(t), \mathbf{u}_2(t), \ldots, \mathbf{u}_{2N-2}(t)$, along with infinitely many zero eigenvalues and corresponding null-space eigenvectors. In light of this, we can rewrite the Hessian at the control landscape maximum in terms of its nonzero spectrum:

$$\mathcal{H}(t,t') = -\sum_{i=1}^{2N-2}|\sigma_i|\mathbf{u}_i(t)\mathbf{u}_i^{\dagger}(t'). \quad (23)$$

Since the trace of the Hessian is bounded by the relation in Eq. (15), as the dimension N increases, each individual nonzero eigenvalue will likely take on an even smaller value, falling off on average as $\sim 1/(2N-2)$. Physically, this means that as higher-energy nuclear eigenstates are included, the curvature of the control landscape in the vicinity of a perfect control solution will likely become flatter, leading to a broader region for which an excellent transition yield can be achieved. Furthermore, this analysis implies that a small perturbation in the control field (e.g., due to laboratory noise) will generate a deviation $\delta P_{i\to f}$, whose magnitude is bounded. By the same argument, this inherent robustness should increase, or at least remain neutrally stable, as the dimension of the nuclear system N increases. In conclusion, the preceding analysis reveals the existence of remarkably attractive quantum control landscapes for laser-driven nuclear transitions where search efforts encounter gentle slopes and maxima that are relatively flat and robust to control field variations.

TABLE I. Important issues for direct quantum control of nuclear dynamics in the laboratory.

Issue	Features
Complexity of nuclear dynamics	(i) The Hamiltonian is not fully or precisely known. (ii) Optimal control fields cannot be effectively designed *a priori* but may be discovered in the laboratory.
Laser specifications	(i) Nuclear energy level spacings are generally much greater than 5 keV (i.e., in the hard x-ray or γ-ray energy range). (ii) Small nuclear transition dipole elements demand exceptionally high laser intensities in order to achieve significant transition amplitude manipulation within the excited state lifetime [2,23].
Pulse engineering	(i) Narrow nuclear transition linewidths (typically on the order of 10^{-6} eV or less [15]) imply that arbitrary manipulations of transition amplitudes would likely require several distinct radiation sources. (ii) Both magnetic and electric fields need consideration.
Transition yield detection	Determining the success of a laboratory control experiment necessitates an appropriate probe of the excited state population.

V. EXPERIMENTAL PROSPECTS

Having established the theoretical groundwork above for direct nuclear excitation control, we now consider the practical aspects of nuclear transition probability manipulation that will be relevant for eventual laboratory implementation. While the theoretical underpinnings of direct laser-driven nuclear control are a natural extension of the analogous atomic and molecular control concepts, many of the traditional experimental approaches to coherent control are not applicable due to both the magnitude of the couplings between nuclear states and the transition energies. As such, significant technological challenges remain before experimental realization of these direct control concepts. This section presents a heuristic overview of the laboratory techniques directly pertinent to nuclear quantum control. Table I first summarizes some of the relevant issues for laboratory quantum control of nuclei.

Some currently available experimental techniques and potential future solutions to the systemic and technological challenges for direct nuclear control are enumerated in Table I and discussed below.

(1) *Complexity of nuclear dynamics*. In order to design an optimal control field *a priori*, detailed knowledge regarding nuclear structure, radiation-matter coupling, and excited state lifetimes is necessary. While the energetics and transition cross sections of nuclei have been studied with γ-ray spectroscopy, unforeseen state couplings or splittings can render theoretically designed fields incomplete or insufficient. As a result, such technical limitations can produce systematic errors in the field design, which may degrade the success of the envisaged control outcome. Alternatively, it is possible to allow the optimal field to be discovered in the laboratory, rather than calculated, through a recursive set of feedback experiments [24]. In this fashion, the measured response of the nuclear system to a trial field serves as input for a pattern-recognition algorithm that can identify attributes of the pulse necessary for accomplishing the desired effect and thus suggest improved fields until a sufficient response is attained.

Following thelatter logic, adaptive feedback control (AFC) implements a closed-loop, adaptive learning strategy in the laboratory and has been broadly applied for the optical control of chemical, physical, and biological systems [5]. In this approach, a set of (often random) initial trial pulse shapes is first crafted and applied to the quantum system. The resultant signal corresponding to each field (e.g., radiative emission from the target state) is subsequently detected, and its overall strength provides a measure of the efficacy of the field. All but the most successful fields are discarded (i.e., through selection pressure), and an evolutionary algorithm subsequently designs a new generation of candidate solutions based upon attributes of the selected successful fields. This new collection of trial fields is then introduced into the sample, and the feedback process leading to iterative refinement of the optimal field continues until a reasonable convergence criterion is reached. The defining advantage of this strategy is that only the most rudimentary knowledge of nuclear transition energies and state couplings are needed in order to properly select the laser frequencies. The adaptive learning process is model free and thus incorporates all available state-to-state couplings, dipolar and otherwise. Additionally, the algorithm automatically adapts the pulse form to account for any experimental uncertainties between the photon source and target.

Successful utilization of AFC is predicated upon a high duty cycle of laser operation and signal acquisition. For instance, the Linac Coherent Light Source (LCLS) at the Stanford Linear Accelerator Center (SLAC) generates hard x-ray laser pulses at a repetition rate of 120 Hz [25]. Similarly, the planned European x-ray free-electron source (XFEL) will operate at 27 kHz [26]. These repetition rates are favorable for adaptive feedback control techniques, provided that signal integration times are reasonable (see forthcoming discussion).

(2) *Laser specifications*. Although most nuclear excited states lie at energies well beyond the accessible range of any near-future laser sources, several nuclei possess long-lived (microseconds to nanoseconds), excited states within approximately 10 keV of the ground state, which corresponds to a photon wavelength of $\lambda \simeq 0.12$ nm. Such hard x-ray photons are only currently available with free-electron laser (FEL) sources. Yet, even with photon sources that enable

resonant interaction, very high peak intensities are necessary in order to overcome the intrinsically small interaction dipoles. Last, as with all coherent control experiments, the field action must be exerted on a coherent time scale for the system. Consequently, ultrafast, high-intensity, coherent hard x-ray light sources are obligatory for direct nuclear quantum control.

Several currently available and planned free-electron laser sources are able to resonantly drive nuclear transitions below 10 keV. For instance, the currently functioning LCLS source at SLAC can operate over the window $0.15\ \text{nm} \lesssim \lambda \lesssim 1.5\ \text{nm}$, which enables direct excitation of nuclear transitions below 8.2 keV [25]. Likewise, the XFEL facility will be able to produce a maximum photon energy of 12.4 keV ($\lambda = 0.1$ nm). The photon energy of these facilities is broadly tunable through adjustment of both the electron beam energy and the magnetic field strength of the undulator. Thus, any nuclear transition in the interval 1–10 keV can be directly accessed with these sources.

Due to the extraordinarily short length scales inherent in nuclei (on the order of 10^{-15} m), direct radiation-matter coupling strengths are quite small. Consequently, in addition to the requisite hard x-ray photon sources, very high laser intensities are concurrently mandatory to efficiently populate nuclear excited states. For example, the peak electric field E_0 necessary to directly induce a complete, resonant population transfer between the ground state and the target excited state (i.e., a π pulse) is given by $E_0 = \pi\hbar/\mu_1\tau$, where τ is the pulse duration, and the transition electric dipole moment μ_1 is on the order of 10^{-34} C m. Assuming a $\tau \simeq 100$ fs pulse, this inversion is achieved with an electric field strength of $E_0 \sim 3 \times 10^{13}$ V/m, which corresponds to a peak intensity of $I_0 \sim 1 \times 10^{20}$ W/cm^2. The laser radiation at LCLS is capable of delivering a peak power of 8 GW at $\lambda = 0.15$ nm [25]. A focal diameter of 2 μm is readily achievable with beryllium lenses at the facility, which provides a peak intensity of $I_0 = 2.5 \times 10^{17}$ W/cm^2. Although less than the intensity necessary for full inversion, this peak intensity would permit meaningful control within the perturbation limit.

One possibility for further intensity augmentation is acceleration of the target nuclear ion into the control laser beam at relativistic velocities [2,4,27]. In the rest frame of the nucleus, the control electric field strength is augmented to $E_N = \sqrt{(1+\beta)/(1-\beta)}E_0$, where $\beta = v/c$ (Lorentz transformation of the electric field). Hence, the pulse peak intensity in the nuclear rest frame is increased to $I_N = [(1+\beta)/(1-\beta)]I_0$. Target acceleration also blueshifts the perceived photon frequency ν_N in the nuclear frame via the relativistic Doppler shift to $\nu_N = \sqrt{(1+\beta)/(1-\beta)}\nu_0$. Thus, target acceleration into the x-ray pulse potentially allows for the driving of nuclear transitions with resonant energies higher than 10 keV; alternatively, target acceleration enables the use of more modest photon energies (e.g., 780-nm Ti:sapphire laser pulses) to resonantly excite low-lying nuclear states. In addition to increasing the effective laser-pulse intensity, the parameter β may be chosen so that the blueshifted photon frequency matches the resonant energy of a desired transition. However, in addition to the increase in experimental complexity incurred by ion acceleration, the use of an ion beam instead of a solid foil target decreases the target number density by orders of magnitude, which dramatically increases the signal acquisition time.

The pulses generated by free-electron laser systems are naturally ultrashort ($\tau \lesssim 100$ fs), which stems from the high gain associated with a spatially compressed electron bunch. As a result, all of the x-ray photons may be delivered to the nucleus on a coherent time scale. Because the radiation of a free-electron laser builds up from noise (self-amplified spontaneous emission) rather than a coherent seed, the temporal characteristics of the pulse are somewhat chaotic, and as a result, these x-ray pulses possess a coherence time shorter than the actual pulse duration. For instance, the x-ray pulses at the LCLS facility consist of several hundred individual spikes whose temporal structure varies on a shot-to-shot basis [25]. Consequently, such rapid decoherence may affect both the degree of quantum system control and, upon averaging, produces a blurred image of the control landscape structure.

Finally, we note that the first excited nuclear state of thorium-229 ($^{229}_{90}$Th) lies only 7.6 eV above the ground state [28]. Direct population of this state through a $M1$ transition could potentially be controlled with up-converted, shaped femtosecond light sources. Since this excitation energy is below the second ionization energy of atomic thorium, it should be possible to probe the nuclear excitation probability through observation of the electronic hyperfine spectroscopic structure. Unfortunately, however, ultraviolet emission from this nuclear excited state has not been directly observed, which currently precludes estimating the requisite control field strengths.

(3) *Pulse engineering*. The implementation of AFC methodologies is incumbent upon the availability of pulse-shaping technology in the spectral region of interest. The vast separation of energy levels ($\Delta E \simeq 10$ keV) that characterize nuclear shell levels renders excitation of multiple eigenstates (e.g., ladder climbing) within the pulse bandwidth impossible with currently envisaged sources. Furthermore, the extraordinarily high field strengths already necessary for one-photon interaction practically dismiss the possibility of multiphoton excitation. Hence, initial direct nuclear control studies would likely entail simple goals within an effective two-level system and might include efficient population transfer or an extension of nuclear spin techniques (NMR) to the realm of nuclear shell excitation for the creation of coherences. Concentrating only on two-level systems also eliminates the complexities of $E1$ and $M1$ transitions simultaneously driven by the same control field. Accordingly, the creation of pulse sequences with a variable number of subpulses and spacings is of prime interest.

Electrons are injected into the LCLS accelerator from a photocathode driven by a frequency-tripled 780-nm Ti:sapphire laser pulse [25]. Although high electron peak currents are necessary for efficient gain in the undulator, the initial electron bunches are not created with a spatial extent equal to that of the final x-ray pulse length (i.e., $\sim$30 μm for a 100-fs pulse); rather, they are created with a much larger spatial extent (approximately 3 mm, corresponding to a $\sim$10-ps excitation pulse) in order to avoid space-charge effects, and the electron bunch is spatially recompressed to the final width with a magnetic chicane only after reaching relativistic velocities. It is relatively straightforward to temporally sculpt laser-pulse sequences consisting of multiple subpulses, each of several picoseconds duration. Since the longitudinal photoelectron

distribution basically follows that of the exciting laser pulse, it should be feasible to extend well-established Ti:sapphire pulse-shaping methodologies for the creation of multiple electron bunches with set spatial separations. Upon entering the undulator, this controlled spatial distribution of electron bunches is translated into an x-ray pulse sequence. Toward this end, the LCLS is already developing the capability to create multiple electron bunches with variable delays. While x-ray pulse sequences with variable delay can be generated with the front-end photoinjection system, pulse shaping of the Ti:sapphire drive laser is not able to control the relative phase between the eventual x-ray subpulses. Yet, due to the diminished coherence time even within a single x-ray pulse, this constraint is likely of minimal consequence.

While indirect x-ray pulse shaping is feasible, all of the experimental constraints (e.g., finite bandwidth, fixed central photon energy, limited temporal coherence, etc.) will likely force a distorted path over the intrinsic nuclear control search landscape described in Sec. IV. Realization of nuclear control may entail an interplay between coherent and incoherent (e.g., optimal temporal energy deposition) control strategies. As such, utilization of evolutionary-guided adaptive feedback control strategies will likely be necessary for arbitrary manipulation of nuclear excitation probabilities.

(4) *Transition yield detection*. The relative degree of excitation into the targeted nuclear state is most readily determined through observation of radiative emission (i.e., x-rays or γ-rays) from that state. Coherent atomic and molecular control experiments are generally unable to ascertain absolute transition yields and rather seek to increase the relative transition probability. Similarly, x-ray or γ-ray emission provides a convenient means for assessing the relative success of a pulse shape in exciting the target state, and laser-driven nuclear control would seek to increase radiative emission from the target state as much as possible.

As outlined above, incorporation of AFC strategies relies on signal acquisition (e.g., detection of the radiative emission) in a timely manner. An order of magnitude estimate of this emitted photon flux is possible utilizing parameters of existing free-electron laser systems. Assuming coherent excitation of the nuclear ensemble (i.e., the pulse duration is significantly shorter than either the dephasing or relaxation time), a transition electric dipole moment of about 10^{-34} C m, and a maximum peak intensity of $I_0 \simeq 2.5 \times 10^{17}$ W/cm^2 (LCLS parameters), the transition yield for resonant nuclear excitation is $P_{i\rightarrow f} \sim 2.4 \times 10^{-3}$. If an atomic nucleus is chosen such that the lowest-energy transition is directly accessible with the x-ray photon energy ($h\nu \lesssim 8.2$ keV), a solid foil sample may be utilized, which has a volume density of about 10^{22} nuclei/cm^3. With a spot diameter of 2 μm at the laser focus and a foil thickness of 1 μm, approximately 3×10^{10} nuclei interact with the x-ray pulse. Correspondingly, $\sim 7 \times 10^7$ nuclei are excited into the first excited shell state per laser pulse. Assuming a laser repetition rate of 120 Hz and a radiative emission yield of 1.0, $\sim 3 \times 10^9$ x-ray photons are emitted each second. With a reasonable detector, this photon flux should permit incorporation of adaptive feedback control methodologies on an acceptable time scale.

Due to the fact that the emitted radiation occurs at the same wavelength as the control pulse, time separation of these two signals is necessary; however, since nuclear states are generally long-lived ($\tau_{1/2} \sim$ ns), it is straightforward to separate the emitted γ rays or x rays from the excitation pulse with time gating of the detector. Finally, as alluded to above, for instances in which the nuclear excitation pulse does not ionize every electron, a time-delayed probing of the electronic-nuclear hyperfine splittings may provide a metric of the efficiency of the nuclear excitation.

VI. CONCLUSIONS

In summary, this work examined the plausibility of direct optimal manipulation of laser-driven nuclear transitions within the context of quantum control. Specifically, the theoretical formalism for coherent control of atomic and molecular systems was extended to nuclear transitions. With the aid of a connectivity graph analysis, the controllability of nuclear systems utilizing both electric dipole and magnetic dipole transitions was demonstrated. Upon establishing the likely controllability of nuclear dynamics, the generic topology of the control landscape was examined. The analysis revealed that in the case of unconstrained controls, the landscape possesses only critical values that correspond to perfect or null control. Accordingly, under unconstrained conditions, climbing the landscape to a global maximum in the laboratory entails navigating a fitness landscape with no hindering suboptimal traps. Due to the large landscape Hessian null-space, the quantum control of nuclei enjoys intrinsic robustness to noise in the immediate vicinity of an optimum. Collectively, these results imply that the transition probability landscape is very attractive for performing experimental optimal nuclear control.

After establishing these theoretical foundations, we addressed the various technological hurdles that must be overcome in order to implement the principles of nuclear quantum control in the laboratory. While existing free-electron laser facilities are able to resonantly interact with nuclear transitions below 10 keV, implementation of high-yield adaptive feedback control is not currently feasible due to limits on both the peak pulse intensities and the capability for creating arbitrary x-ray pulse sequences. Nonetheless, fundamental studies exploring the direct interaction of energetically accessible nuclear two-level systems with ultrafast x-ray pulses is presently possible. Such studies would provide the groundwork for future control experiments as laser-pulse-shaping capabilities and temporal coherence improve.

Due to the extreme photon energies and field strengths necessary for direct interaction, present nuclear studies utilize laser-accelerated high-energy particles (e.g., electrons, protons, and neutrons) or Bremsstrahlung radiation to indirectly induce nuclear excitations and reactions with resonant energies as high as several tens of MeV, including photodisintegration and fission [3]. A basic distinction from the work in this paper is that these interactions (radiation matter or collisional) are incoherent. Yet it has been demonstrated that quantum control may also operate in this regime dominated by incoherent interactions [29], and the use of incoherent optimal control for even modest increases in the yield of these relatively low-efficiency processes would create important opportunities for the study and manipulation of high-energy nuclear dynamics and merits further study. Of particular interest is

the possibility of controlling the population or depopulation of long-lived isomeric states, which may provide a pumping mechanism for γ-ray lasers as well as the means to store energy in nuclear batteries (see [30] for example). Incoherent control strategies may also lead to increased photodisintegration and fission yields, with important applications such as the neutralization of hazardous radioactive waste and prospective next-generation energy sources [31]. Incorporation of incoherent control strategies will also be beneficial in the context of direct laser control since currently available x-ray photon sources exhibit limited temporal coherence. In the end, efficient manipulation of nuclear dynamics will likely rely on an amalgam of coherent and incoherent control techniques.

In conclusion, the proposed extension of coherent control methodologies to the nuclear scale offers an attractive framework for driving laser-induced nuclear excitations. Such studies should also provide a means for increased understanding of the structure and dynamical evolution of the atomic nucleus.

ACKNOWLEDGMENTS

The authors acknowledge support from the Department of Energy. The authors are also grateful to Dr. Ronald Davidson for reading the manuscript and providing constructive feedback.

[1] T. J. Bürvenich, J. Evers, and C. H. Keitel, Phys. Rev. Lett. **96**, 142501 (2006).
[2] T. J. Bürvenich, J. Evers, and C. H. Keitel, Phys. Rev. C **74**, 044601 (2006).
[3] H. Schwoerer, J. Magill, and B. Beleites, *Lasers and Nuclei* (Springer, Heidelberg, 2006).
[4] A. B. Pálffy, J. Mod. Opt. **55**, 2603 (2008).
[5] C. Brif, R. Chakrabarti, and H. Rabitz, New J. Phys. **12**, 075008 (2010).
[6] C. Chen, Y. Y. Yin, and D. S. Elliott, Phys. Rev. Lett. **64**, 507 (1990).
[7] H. G. Muller, P. H. Bucksbaum, D. W. Schumacher, and A. Zavriyev, J. Phys. B **23**, 2761 (1990).
[8] B. Sheehy, B. Walker, and L. F. DiMauro, Phys. Rev. Lett. **74**, 4799 (1995).
[9] N. F. Scherer, R. J. Carlson, A. Matro, M. Du, A. J. Ruggiero, V. Romero-Rochin, J. A. Cina, G. R. Fleming, and S. A. Rice, J. Chem. Phys. **95**, 1487 (1991).
[10] E. Hertz, O. Faucher, B. Lavorel, and R. Chaux, J. Chem. Phys. **113**, 6132 (2000).
[11] E. Dupont, P. B. Corkum, H. C. Liu, M. Buchanan, and Z. R. Wasilewski, Phys. Rev. Lett. **74**, 3596 (1995).
[12] P. Ring and P. Schuck, *The Nuclear Many-Body Problem* (Springer, New York, 1980).
[13] M. K. Pal, *Theory of Nuclear Structure* (Affiliated East-West Press, New Delhi, 1981).
[14] M. A. Preston and R. K. Bhaduri, *Structure of the Nucleus* (Addison-Wesley, Reading, MA, 1975).
[15] W.-T. Liao, A. Pálffy, and C. H. Keitel Phys. Lett. B **705**, 134 (2011).
[16] S. G. Schirmer, H. Fu, and A. I. Solomon, Phys. Rev. A **63**, 063410 (2001).
[17] The Evaluated Nuclear Structure Data File (ENSDF) database [http://www.nndc.bnl.gov/ensdf/].
[18] R. Wu, H. Rabitz, G. Turinici, and I. Sola, Phys. Rev. A **70**, 052507 (2004).
[19] Z. Shen, M. Hsieh, and H. Rabitz, J. Chem. Phys. **124**, 204106 (2006).
[20] H. Rabitz, T.-S. Ho, M. Hsieh, R. Kosut, and M. Demiralp, Phys. Rev. A **74**, 012721 (2006).
[21] T.-S. Ho and H. Rabitz, J. Photochem. Photobiol. A **180**, 226 (2006).
[22] A. Rothman, T.-S. Ho, and H. Rabitz, Phys. Rev. A **73**, 053401 (2006).
[23] S. Matinyan, Phys. Rep. **298**, 199 (1998).
[24] R. S. Judson and H. Rabitz, Phys. Rev. Lett. **68**, 1500 (1992).
[25] LCLS: Linac Coherent Light Source [http://ssrl.slac.stanford.edu/lcls/cdr/].
[26] M. Altarelli *et al.*, XFEL: The European X-Ray Free-Electron Laser. Technical Design Report, DESY, Hamburg (2006).
[27] A. B. Pálffy, J. Evers, and C. H. Keitel, Phys. Rev. C **77**, 044602 (2008).
[28] B. R. Beck, J. A. Becker, P. Beiersdorfer, G. V. Brown, K. J. Moody, J. B. Wilhelmy, F. S. Porter, C. A. Kilbourne, and R. L. Kelley, Phys. Rev. Lett. **98**, 142501 (2007).
[29] A. Pechen and H. Rabitz, Phys. Rev. A **73**, 062102 (2006).
[30] C. B. Collins, J. J. Carroll, T. W. Sinor, M. J. Byrd, D. G. Richmond, K. N. Taylor, M. Huber, N. Huxel, P. von Neumann-Cosel, A. Richter *et al.*, Phys. Rev. C **42**, R1813 (1990).
[31] K. W. D. Ledingham and W. Galster, New J. Phys. **12**, 045005 (2010).